Measurement of a complete set of analyzing powers and cross section of the kinematically complete breakup reaction $^4\mathrm{He}(\vec{d},p\alpha)n$ at 7.0 MeV and the isospin-forbidden d^*

P. Niessen, S. Lemaître, K. R. Nyga, G. Rauprich, R. Reckenfelderbäumer, L. Sydow, and H. Paetz gen. Schieck
Institut für Kernphysik, Universität Köln, D-5000 Köln 41, Germany

P. Doleschall
Central Research Institute for Physics, H-1525, Budapest 114, Hungary
(Received 4 October 1991)

The breakup reaction $^4\mathrm{He}(\vec{d},p\alpha)n$ at $E_d=7.0$ MeV has been investigated in a kinematically complete experiment with vector and tensor polarized deuterons in a kinematical situation with zero relative energy of the two outgoing nucleons, a preferred situation to show effects from the singlet deuteron d^* and therefore isospin breaking. A complete set of analyzing powers, A_y, A_{yy}, A_{xz}, and A_{zz} in addition to the differential breakup cross section, $d^3\sigma/d\Omega_3 d\Omega_4 dS$ has been measured. The data are compared to new Faddeev calculations including an approximate (cutoff) Coulomb potential allowing for the d^* production and also D-wave α-N interactions. Good agreement is found for the polarization observables and the shape of the cross section which, however, disagrees in absolute magnitude. Both the inclusion of the d^* and of D waves seem necessary for a good description of all data and for the interpretation of a small excursion in some observables in the n-p final-state interaction region as a manifestation of the isospin-forbidden d^*.

PACS number(s): 25.10.+s, 24.70.+s, 25.45.−z, 24.80.−x

I. INTRODUCTION

The α-d six-nucleon system is one of the few many-body systems for which Faddeev calculations are hoped to be applicable by reducing it to a three-body problem of the α particle and the two nucleons. In this way the α-d or α-p-n scattering system (elastic scattering and breakup reaction) have been treated quite successfully. Experimental results have shown that this is a valid concept, at least as long as the incident energy is not too high (e.g., $E_{\mathrm{c.m.}} \leq 20$ MeV). The more recent calculations by Koike [1,2] and Doleschall [3] used separable approximations with Yamaguchi or generalized Yamaguchi-type form factors for the potentials describing the α-N and the p-n interactions. States up to the $S_{1/2}$, $P_{1/2}$, and $P_{3/2}$ partial waves were used for the α-N system and $^3S_1$ only for the p-n interaction. The n-p tensor force has also been introduced in different approaches. Its inclusion appeared necessary especially for a good description of second-rank analyzing powers [4].

One unsolved problem is the treatment of the long-range Coulomb interaction mainly due to computational difficulties. Only approximate treatments have been attempted so far, such as the introduction of a final-state correction to the p-α t matrix only [2], or—more realistically—by introducing a repulsive potential barrier with a height of 0.5 MeV in the intermediate range of 4–10 fm into the Faddeev equations (Doleschall's model M2) [3,5].

The Coulomb problem is intimately connected with the question of isospin-forbidden production of the d^* (the $^1S_0$ state of the p-n system) in the reaction $^4\mathrm{He}(d,p\alpha)n$ in a final-state interaction (FSI). Since the Coulomb interaction breaks the conservation of isospin, the manifestation of d^* in this reaction could naturally be explained if a Coulomb interaction, and therefore an explicit difference between the p-α and the n-α interactions, could be introduced in the three-body calculations. A more microscopic approach would have to take into account some charge-symmetry breaking, e.g., on the meson-exchange or quark level.

Several experimental attempts have been made to find clear evidence for a transition to the d^* in this breakup reaction [6–8]. The experiment of [8] was specifically optimized to look for the d^* by measuring the tensor analyzing power A_{yy} at the lowest practicable incident energy of 7.0 MeV. It was performed in one kinematical situation, i.e., at laboratory angles $\theta_3(\alpha)=32°$ and $\theta_4(p)=62°$, corresponding to a d^* c.m. emission angle of 100.9°, with an n-p final-state interaction which had predicted in a simple model calculation a strong effect of d^* [9]. Another quantity which should be sensitive to the d^* production, namely, the substate cross section $\sigma(m=0)$ for deuterons in the $m=0$ substate, was derived from A_{yy} and the (spin-averaged) differential breakup cross section. Both A_{yy} and $\sigma(m=0)$ showed a clear excursion, in contrast to $\sigma(m=\pm 1)$, which was taken as a clear sign of d^* production by the authors.

It is certainly useful to search for additional evidence of isospin-forbidden d^* production. One should also test new improved Faddeev calculations, which allow for a difference between α-n and α-p caused by an approximate Coulomb interaction, and therefore for isospin breaking. Therefore, a complete set of vector and tensor analyzing

powers (A_y, A_{zz}, A_{yy}, and A_{xz}) and the differential cross section have been measured in a different p-n FSI configuration (i.e., for a c.m. d^* production angle of 70°). In Sec. IV, the results are compared to the new Faddeev calculations discussed in detail in Sec. III.

II. EXPERIMENT

A. Choice of the kinematical situation

The present experiment was chosen after considering several experimental goals: an n-p FSI configuration (with $E_{n\text{-}p}=0$) with a large d^* production probability as predicted by [9], but sufficiently distinct from the situation of Ref. [8] and also well separated from resonant N-α FSI enhancements (e.g., ^{5}He), an energy as low as technically possible to enhance any Coulomb effects—the limit was given by an experimental spread of the data around the kinematical curve so large that the curve could not be determined (this was tested at several energies below $E_d=7.0$ MeV), finally, the possible gain in statistical accuracy and partial elimination of experimental asymmetries by a left-right symmetrical detector arrangement. Therefore, an incident energy of $E_d=7.0$ MeV and symmetric detector angles of $\theta_3=\theta_4=42°$ both left and right of the beam ($\Phi_{3,4}=0°$ and 180°) were chosen.

B. Experimental setup

Two Si surface barrier detectors were mounted in an ORTEC2800 scattering chamber. The vector or tensor polarized beam from the polarized ion source LASCO was accelerated by the Cologne FN tandem Van de Graaff accelerator to 7.0 MeV. The orientation of the polarization could be changed to any direction by the rotatable Wien filter on the source. The vector polarization was measured in intervals by moving the two detectors to $\theta_3=\theta_4=50°$ (left and right) where the analyzing power is large, well known, and relatively angle independent [10]. Then the detectors were moved back to 42°, the polarization was measured again and monitored continuously during the coincidence measurements. The vector polarization was $\hat{p}=0.45\pm0.02$. The tensor polarization was measured at intervals in a separate scattering chamber in the beam line using the ^{3}He(d,p)^{4}He reaction at 0° (after rotating the spin quantization axis into the longitudinal direction). The average tensor polarization of the beam was $\hat{p}_{zz}=-0.68\pm0.03$. Both polarizations were constant within these errors during the length of the intervals. Typical beam currents on target were 250 and 350 nA for the tensor and vector polarized beams, respectively.

The scattering chamber was equipped with a beam entrance foil close to the chamber centre (Ni, 1 μm thick) and a large exit foil (Havar, 2.5 μm thick) before the Faraday cup to allow accurate beam current integration. The entire chamber was filled with ^{4}He at a pressure of 80 mbar. The gas-target volume was defined by the beam (focused to a minimal spot of 2–3 mm diameter because of some straggling) and by a double-slit system in front of the detectors. The target pressure was chosen as a compromise between contradictory requirements: relatively large energy loss and straggling especially for the already low-energy α particles, good definition of angles and solid angles, but with solid angles as large as possible, and sufficient flight path of both reaction products to enable the time-of-flight difference discrimination method used (a distance of 2×13 cm was finally chosen).

III. DATA ANALYSIS

The pulses from the detectors were processed in a conventional fast-slow coincidence circuitry and the coincidence events were stored as triples (E_3, E_4, Δt) event by event on magnetic tape together with a status word. Because of the symmetrical detector arrangement, the breakup events in a kinematically complete measurement must appear ideally on two kinematical loci (α-p and p-α) in the E_3-E_4 plane which are mirror images about the diagonal. In reality, these curves are deformed differently by the energy loss, mainly of the α particles. At an energy of 7 MeV, the only interfering reaction on a pure ^{4}He target can be elastic scattering. In the E_3-E_4 plane, a background of accidental coincidences appears as shown in Fig. 1.

For the discrimination of the accidentals as well as the separation of the two partly overlapping kinematical curves, the time-of-flight difference between the two coin-

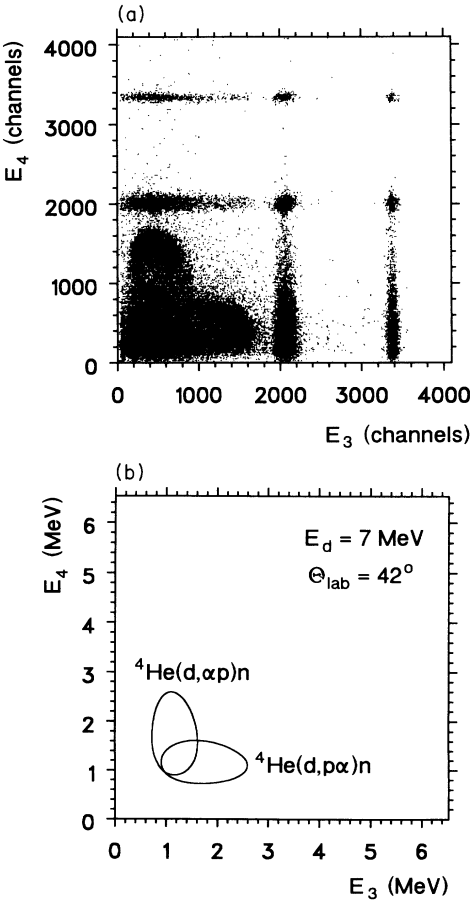

FIG. 1. Typical raw E_3-E_4 spectrum and the spectrum expected from kinematics, but without energy loss.

cident reaction products has been used: see, e.g., [11,12]. In the process of projecting the true coincident events onto the kinematical curves only those events were selected which, by their time-of-flight difference, could be identified as belonging to the class of true coincidences. They appear in a narrow time window in the time-difference spectrum as shown in Fig. 2. A two-dimensional time matrix of the measured time differences ($\Delta t_{\rm exp}$) vs the "theoretical" time difference $\Delta t_{\rm theo}$, calculated from the measured energies E_3 and E_4, the assumed masses m_3 and m_4, and the known flight path length should show the "right" events as a straight line, other events as curved lines from which the true events of the right kind can be separated by a suitable projection perpendicular to the straight line. In our case, because of large energy losses and energy spreads, the true events are spread out appreciably but nevertheless well separated from unwanted events as shown in Fig. 3. The projection onto the kinematical curve was performed only with the events inside the marked area with the additional provision that the effect of subtracting accidental coincidences on the experimental errors could be minimized by choosing a maximally wide window for the background events. Details of the method are described in [13,14].

The projection of the true events onto the kinematical curve and the absolute energy calibration of the spectra meet the difficulty that the energy losses had to be taken into account for constructing the kinematical curve (as well as for the time-of-flight differences). Therefore, the energy losses were calculated including the variations in the gas-target pressure for each run and with these the energies of all events were corrected. The events as well as the kinematical curves were transformed into the momentum plane, where the curve is an ellipse which was transformed conformally into a circle. Events in equal angular intervals around that circle were projected onto it. A retransformation into the energy plane and an absolute energy calibration then projected the yield spectra along the kinematical curve as a function of the arc parameter S (in MeV). With an absolute normalization calculated from the beam intensity, the effective target

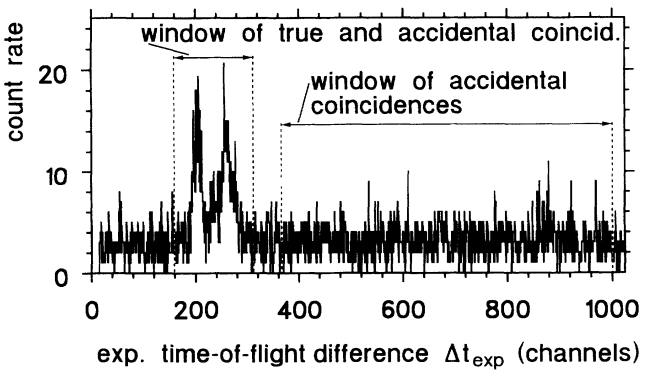

FIG. 2. Typical experimental time-difference spectrum. The two peaks correspond to the two kinematical curves with true events sitting on a background of accidental coincidences.

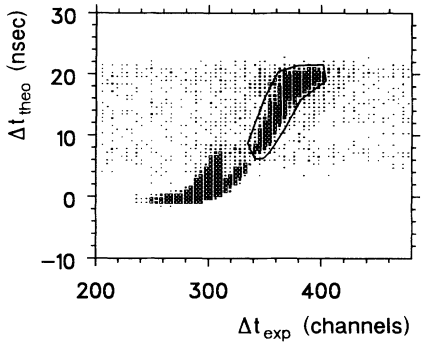

FIG. 3. Typical time-difference matrix with the area of the true p-α events marked by a polygon.

thickness (from the gas pressure and the coincidence volume), and the detector solid angles, the absolute differential breakup cross section

$$d^5\sigma/d\theta_3 d\Phi_3 d\theta_4 d\Phi_4 dS \equiv d^3\sigma/d\Omega_3 d\Omega_4 dS$$

was calculated. From differences of the yield spectra with different beam polarizations, the different analyzing powers were obtained.

The relation between the differential cross section with polarized and unpolarized spin-1 beams in coplanar geometry, assuming parity conservation for a three-particle breakup reaction, is the same as for a two-particle reaction [15–17]. Only four independent analyzing powers remain:

$$\sigma(\theta,\Phi)=\sigma_0(\theta)[\,1+\tfrac{3}{2}p_y A_y+\tfrac{2}{3}p_{xz}A_{xz} +\tfrac{1}{6}(p_{xx}-p_{yy})(A_{xx}-A_{yy})+\tfrac{1}{2}p_{zz}A_{zz}\,]$$

with

$$\begin{aligned} p_y &= \hat{p}\sin\beta\cos\Phi\ , \\ p_{xz} &= -\tfrac{3}{2}\hat{p}_{zz}\sin\beta\cos\beta\sin\Phi\ , \\ p_{xx} &= \tfrac{1}{2}\hat{p}_{zz}(3\sin^2\beta\sin^2\Phi-1)\ , \\ p_{yy} &= \tfrac{1}{2}\hat{p}_{zz}(3\sin^2\beta\cos^2\Phi-1)\ , \\ p_{zz} &= \tfrac{1}{2}\hat{p}_{zz}(3\cos^2\beta-1)\ , \end{aligned} \tag{1}$$

where $\hat{p}$ and $\hat{p}_{zz}$ are the components of the beam vector and tensor polarization relative to the quantization axis, respectively.

In the present experiment where only two detectors in a plane could be used, the polarization was oriented at three different polar angles: $\beta=0°$ was used for the determination of A_{zz}, $\beta=54.7°$ for a combination of A_{xz} and $A_{xx}-A_{yy}$, and $\beta=90°$ for the vector analyzing power A_y and the combination of A_{zz} and $A_{xx}-A_{yy}$. For the tensor analyzing powers, runs using purely tensor-polarized and unpolarized beams with beam current normalization had to be taken. For the vector analyzing power, left-right asymmetries were measured with a purely vector-

polarized beam with spin "up" and "down" without the necessity of charge integration.

From the measured tensor analyzing powers, the quantity A_{yy}, which should be sensitive to d^* production, was extracted. Another sensitive quantity, the substate differential cross section $\sigma^0 \equiv \sigma(m=0)$ and the complementary insensitive quantity $\sigma^{\pm} \equiv \sigma(m=\pm 1)$ can be calculated from the unpolarized differential cross section σ_0 and A_{yy}. Similar to [8],

$$\sigma^0 = \sigma_0(1 - A_{yy}) ,$$
$$\sigma^{\pm} = \tfrac{1}{2}(3\sigma_0 - \sigma^0) . \tag{2}$$

(In [8], $\sigma^{\pm}$ was defined without the factor 1/2.)

IV. THEORY

The first elaborate Faddeev calculations for the $\alpha+p+n$ system were performed by Koike [2]. The results for the breakup process were reasonably good, although at lower energies [below $E_{\text{lab}}(d)=6$ MeV] the calculations failed to reproduce the experimental data at some angle combinations [18]. These disagreements were believed to result mainly from the missing Coulomb interaction, and, consequently, the missing n-p singlet, S-wave interaction. In Koike's model, since the Coulomb interaction was taken into account only as a final-state correction, the n-p singlet S-wave interaction is dropped from the Faddeev equations.

Some attempts were made to imitate the difference of the alpha-neutron and alpha-proton interactions, so the n-p singlet S-wave interaction could be brought into the system [3]. This, however, led to an overestimate of the effects of the n-p singlet S-wave interaction.

The basic purpose of performing a new type of calculation was to try to include more properly the n-p singlet S-wave interaction. Since isospin conservation is broken by the Coulomb force, in order to model properly the effect of the n-p singlet S-wave interaction, the difference between the alpha-neutron and alpha-proton interactions was assumed to originate completely with the Coulomb force. Unfortunately, the Coulomb interaction has a long-range character which could not be included exactly. Therefore, the model applied is a compromise between reality and computational possibilities.

First a phenomenological local potential described the alpha-neutron scattering data in the S-, P- [19], and D-wave [20] channels. The potentials were chosen as a sum of Gaussians

$$V = \sum_{i=1}^{m} \alpha_i \exp[-(\beta_i r)^2] , \tag{3}$$

where $m=4$ was chosen for the P waves and $m=3$ for the D waves. To account for the alpha-particle structure, the local S-wave potential was constructed with a bound state which was then removed by a strong repulsive, rank-1 separable interaction with an oscillator function form factor:

$$V = \delta(r-r') \sum_{i=1}^{3} \alpha_i \exp[-(\beta_i r)^2] + g(r)\lambda g(r') , \tag{4}$$

where

$$g(r) = [2/(\pi^{1/4} R_0^{3/2})] \exp[-0.5(r/R_0)^2]$$

and the parameter values $R_0=1.71$ fm, $\lambda=1000$ MeV were chosen. The other potential parameters are listed in Table I. This potential fits the experimental phase shifts up to 20 MeV very well.

The alpha-proton potentials were created by adding a cutoff Coulomb potential to the alpha-neutron interactions. The shape of this cutoff potential was chosen as

$$V_{\text{cutoff}}^{\text{Coul}} = Z_\alpha Z_p \begin{cases} [3-(r/R_I)^2]/(2R_I) & \text{if } r \le R_I , \\ 1/r & \text{if } R_I \le r \le R_{\text{cutoff}} , \\ (1/r)\exp\{-[a(r-R_{\text{cutoff}})]^n\} & \text{if } r \ge R_{\text{cutoff}} , \end{cases} \tag{5}$$

with the parameter values $R_I=1.5$ fm, $R_{\text{cutoff}}=7.5$ fm, $a=0.30$ fm^{-1}, $n=2$. The cutoff radius R_{cutoff} was chosen large enough to include some of the repulsion outside the range of the nuclear interaction, although this may not be too important for breaking of isospin conservation.

The next step was separable expansion of the local (or partly nonlocal for the $S_{1/2}$ channels) potentials. The

TABLE I. The parameters of the alpha-neutron interaction.

	$S_{1/2}$	$P_{1/2}$	$P_{3/2}$	$D_{3/2}$	$D_{5/2}$
α_i (MeV)	−0.444	−0.287 8	−0.977 21	−1.0	−1.0
	−12.980	−8.973 0	−19.323 00	−586.1	−672.9
	−38.750	−31.250 0	−47.820 00	480.6	628.7
		14.400 0	10.934 00		
β_i (fm^{-1})	0.291 3	0.352 6	0.284 60	0.7	0.700 0
	0.418 9	0.391 4	0.444 57	1.0	0.986 3
	0.582 7	0.441 5	0.497 46	1.5	1.451 0
		0.599 3	0.786 17		

Ernst-Shakin-Thaler (EST) method [21], propagated by the Graz group [22], was chosen with a slight alteration of the method use by Haidenbauer and Plessas. Since, in Faddeev equations, the integration covers predominantly negative energy values of the two-body propagator, the pointwise EST approximation of the original two-body t matrix is made at zero or negative energies (except for the $P_{3/2}$ channels, where the sharp resonance had to be reproduced). In this procedure we found that a simple rank-2 separable approximation is an excellent approach for the alpha-neutron interactions if we require the reproduction of the phase shifts, produced by the original potentials, at least up to 20 MeV. For the D-wave interactions, the agreement is even satisfactory up to 150–200 MeV.

The separable approximation of the alpha-proton interaction proved more difficult because of the longer range of the added cutoff Coulomb potential. To obtain accuracy similar to that for the alpha-neutron interaction, rank-4 separable approximations have to be chosen (although we accepted a slightly worse quality for the D-wave interactions, where rank-3 approximations were used). The fixed energies and momenta used in the EST separable approximations are listed in the Table II. The neutron-proton interaction was chosen to be the rank-1 separable approximation of the Paris potential by Haidenbauer and Plessas [22]. An earlier unpublished calculation, where the rank-3 singlet S-wave interaction and the rank-4 triplet coupled S- and D-wave interactions of Ref. [22] were applied together with the S- and P-wave alpha-nucleon interactions, gave no significant difference from calculations with the rank-1 neutron-proton interactions. This may not be true if the D-wave alpha-nucleon interactions are also included, but as a first approach the use of the rank-1 neutron-proton interactions seems reasonable.

Faddeev calculations were performed using the above-listed separable interactions. Four sets of calculations were performed in order to see the effect of the different parts of the interactions. The basic calculation was a Koike-type calculation. In the sense that only the S- and P-wave alpha-nucleon and the S-D neutron-proton tensor force were included. The alpha-neutron and alpha-proton interactions were different and both the ^{5}Li and ^{5}He resonances have their proper positions already in the Faddeev equations.

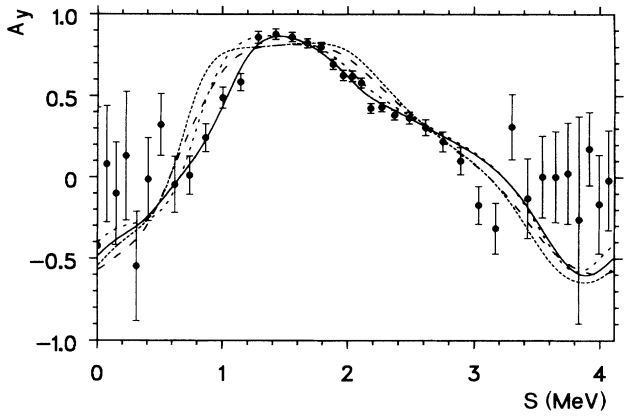

FIG. 4. Vector analyzing power $A_y(\theta_3,\Phi_3,\theta_4,\Phi_4,S)$ of the ^{4}He$(\vec{d},p\alpha)n$ reaction at $E_d=7.0$ MeV and $\theta_3=\theta_4=42°$, $\Delta\Phi_{3,4}=180°$ as a function of the arc length parameter S (MeV). The region of d^* is around $S=0.9$ MeV, the α-n FSI regions are around $S=1.7$ and 2.5 MeV. The lines are theoretical predictions. Small, closely spaced dashes; basic calculation (S- and P-wave α-N and S-D n-p tensor force), small, widely spaced dashes, α-N D waves additionally included, large dashes, basic calculation with the S-wave n-p interaction additionally included, solid line, full calculation with α-N D wave *and* singlet S-wave n-p interaction.

In the second calculation we included the D-wave alpha-nucleon interactions. A significant effect was found.

The next two calculations already include the singlet S-wave neutron-proton interaction: one without and one with the D-wave alpha-neutron interactions. In the n-p FSI region, the relatively weak effect of the singlet S-wave n-p interaction alone is quite similar to the effect of including the D waves alone for all observables, whereas the inclusion of both makes significant changes in the region of d^*.

TABLE II. The energy and momentum values for the EST separable expansion. The energies and the squared momenta are given in MeV. Negative energy values, c.m. energies; positive values, the usual nucleon laboratory energies.

		E_1	p_1^2	E_2	p_2^2	E_3	p_3^2	E_4	p_4^2
α-n									
	$S_{1/2}$	−5.0	5.0	−25.0	25.0				
	$P_{1/2}$	0.0	0.0	−20.0	20.0				
	$P_{3/2}$	1.2	1.2	−8.0	8.0				
	$D_{3/2},D_{5/2}$	0.0	0.0	−200.0	200.0				
α-p									
	$S_{1/2}$	0.0	0.0	−2.0	2.0	−8.0	8.0	−25.0	25.0
	$P_{1/2}$	0.0	0.0	−2.0	2.0	−8.0	8.0	−20.0	20.0
	$P_{3/2}$	2.5	2.5	0.0	0.0	−4.0	4.0	−12.0	12.0
	$D_{3/2},D_{5/2}$	0.0	0.0	−7.0	7.0	−200.0	200.0		

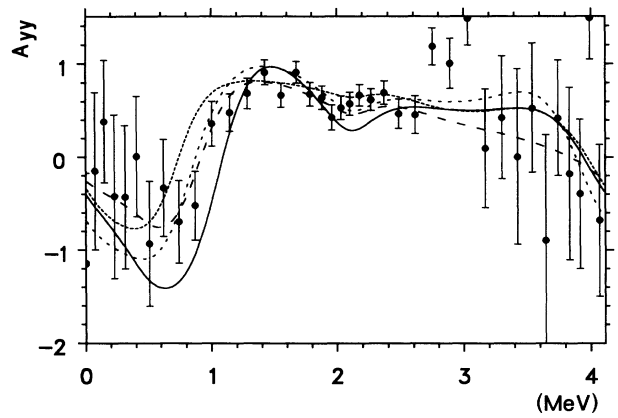

FIG. 5. Same as Fig. 4, but for the tensor analyzing power A_{yy}.

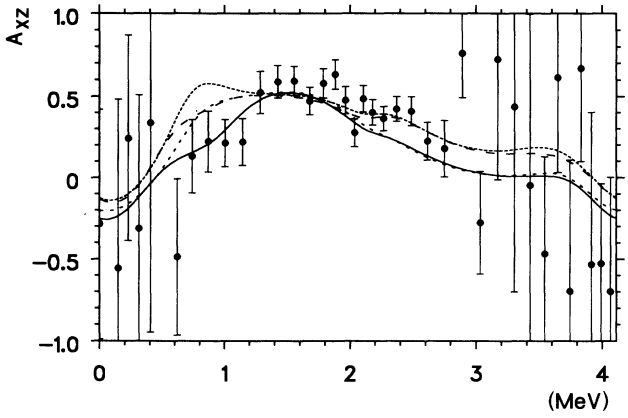

FIG. 7. Same as Fig. 4, but for the tensor analyzing power A_{xz}.

Because of the significant effect of the alpha-nucleon D-wave interactions and the presence of the singlet S-wave n-p interactions caused by inclusion of the cutoff Coulomb force, only the calculation with all interactions should be considered when comparing with experimental data.

V. RESULTS AND DISCUSSION

In Figs. 4–10, the experimental results are shown together with the new Faddeev calculations in the following order: differential breakup cross section $d^3\sigma/d\Omega_3 d\Omega_4 dS$ in mb/sr^2 MeV, vector analyzing power A_y, the three tensor analyzing powers A_{zz}, A_{xz}, and A_{yy}, as well as the spin substate differential cross sections $\sigma(m=0)$ and $\sigma(m=\pm 1)$, all as functions of the arc length parameter S in MeV. The region of the n-p FSI (d^*) is at $S=0.9$ MeV, whereas the n-α FSI corresponding to the ground state of ^{5}He are at $S=1.7$ and 2.5 MeV and, due to the widths of their resonant cross-section peaks, are not separated experimentally. It should be noted that the cross section is large only in the ^{5}He region, it is quite small in the d^* region. This leads to large errors, especially for the analyzing powers. Only statistical errors are shown in the figures. An additional systematic uncertainty of the absolute magnitude of the cross sections, mainly from uncertainty of the active target volume and the detector solid angles, is estimated to less than 15%. When judging the amount of (dis)agreement of the results with the calculations, it should be noted that, in the region above $S\approx 2$ MeV, the energies of the α particles were close to the limit of detectability beyond which, due to the rather wide scatter of the events around the kinematical locus, a gradual loss of counts cannot be excluded. However, this concerns the cross sections only, since for the analyzing powers equal percentages of events with polarized and unpolarized beams were affected.

The curves shown in all figures are the four variants of the Faddeev calculations: (i) The basic calculation with only S and P waves of the α-N interaction (small, closely spaced dashes); (ii) in addition to the basic input, α-N D waves also are included (small, widely spaced dashes); (iii) the basic calculation is amended by the n-p $^1S_0$ interaction (large dashes); and (iv) the full calculation containing the n-p $^1S_0$ interaction and the α-N D waves in addition

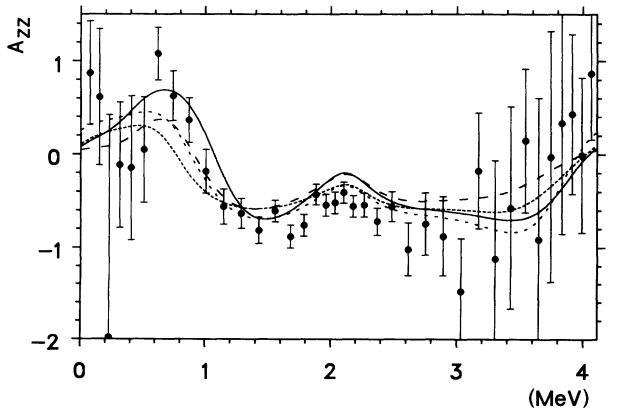

FIG. 6. Same as Fig. 4, but for the tensor analyzing power A_{zz}.

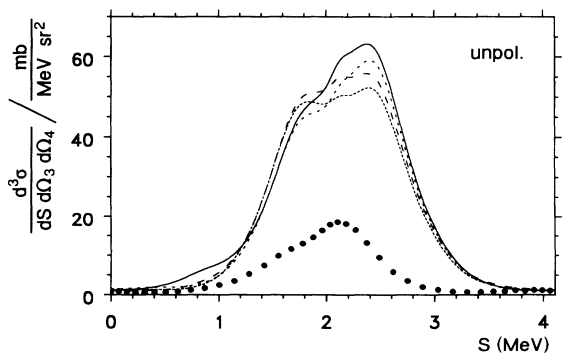

FIG. 8. Same as Fig. 4, but for the differential cross section $d^3\sigma/d\Omega_3 d\Omega_4 dS$.

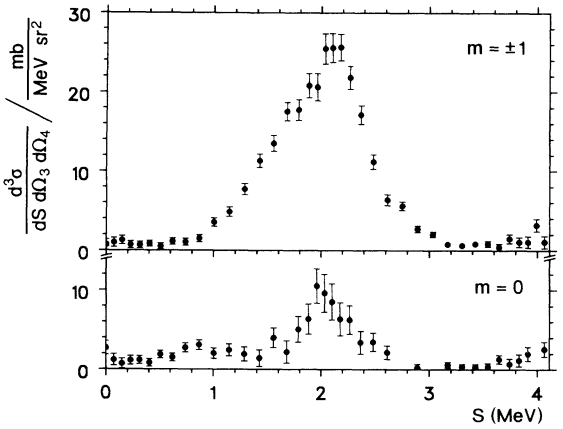

FIG. 9. The experimental spin substate cross sections $\sigma^{\pm}$ and σ^{0} according to Eqs. (2) as functions of the arc length parameter S (MeV). The region of d^* is around $S=0.9$ MeV, the α-n FSI regions are around $S=1.7$ and 2.5 MeV.

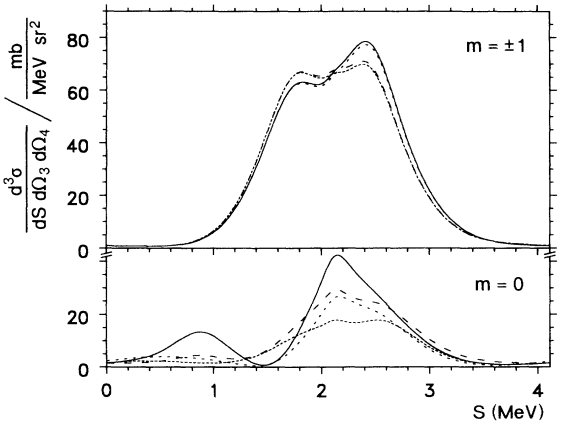

FIG. 10. Theoretical predictions for the spin substate cross sections $\sigma^{\pm}$ and σ^{0}. The different lines have the same meaning as above. The full calculation shows a bump in the region of d^*.

to the basic calculation (solid line). The comparison shows that, for the polarization observables, the general agreement, especially in the central region, with the smaller error bars is quite good. There, however, the four calculations do not differ very significantly. Nevertheless, the full calculation seems to provide the best overall agreement, see, e.g., the vector analyzing power with its relatively small errors. For the differential cross section, the shape is reproduced quite well. The overall magnitude, however, seems to be off by a substantial factor for all four calculations.

In the region of the p-n FSI we note that—within the larger experimental errors—the full calculation gives by far the best description of the observables. It appears, however, necessary to include the D waves in addition to the $^1S_0$ interaction, since without them the changes from the basic calculation are insignificant. Surprisingly, the quantity A_{yy} does not show a drastic effect from $^1S_0$, though the analyzing power moves in the right direction (the value for a pure transition to the $^1S_0$ state would be $A_{yy}=-1$ due to the spin and isospin structure of this reaction; see [8]).

As in [8], the strongest evidence for the transition to d^* comes from the comparison of the spin substate cross sections (Figs. 9 and 10). Only $\sigma(m=0)$ shows a clear bump in the region of d^* whereas $\sigma(m=\pm1)$ is flat there, both in agreement with the shape of the Faddeev calculations and as expected from angular-momentum considerations. The (spin-averaged) unpolarized cross section shows a correspondingly smaller enhancement.

VI. SUMMARY AND OUTLOOK

Comparison between the experimental data of the present experiment and the new Faddeev calculations presented shows that the best overall agreement for the breakup cross section and a set of four analyzing powers is obtained with the full calculation including α-N D waves and the n-p $^1S_0$ interaction. This is especially true for the vector analyzing power. In the region of $E_{n\text{-}p}=0$, where effects of the singlet-deuteron production would be expected, comparison between data and theoretical calculations for the substate cross sections $\sigma(m=0)$ and $\sigma(m=\pm1)$ shows that the reaction mechanism is dominated by the n-p singlet FSI. On the other hand, for the tensor analyzing power A_{yy}, which should be sensitive to the singlet deuteron, there is no clear evidence for an enhancement in this region. However, the n-p FSI especially occurs in a region of rather low cross section and correspondingly large errors.

Both the d^* enhancement in some observables and the improved overall description when including the $^1S_0$ interaction may nevertheless be interpreted as another indication for an isospin breaking in the ^{4}He$(d,\alpha p)n$ breakup reaction in a quasi-two-particle kinematics ^{4}He$(d,d^*)^4$He. This is observed at the same energy but at a different d^* production angle than in the earlier experiment where such evidence had been found.

ACKNOWLEDGMENTS

This work has been partly supported by the German Minister for Research and Technology (BMFT) under the Contract Nos. O6-OK-153 and O6-OK-272. The numerical work has been performed on the CDC Cyber 72/76 of the Regionales Rechenzentrum der Universität zu Köln. The authors want to thank Prof. F. Cannata and Prof. M. Bruno, University of Bologna, for stimulating discussions in the planning phase of the present work and the members of the nuclear reaction group for their help in taking the data.

[1] Y. Koike, Progr. Theor. Phys. **59**, 87 (1978).
[2] Y. Koike, Nucl. Phys. **A301**, 411 (1978); **A337**, 23 (1980).
[3] P. Doleschall, Gy. Bencze, M. Bruno, F. Cannata, and M. D'Agostino, Phys. Lett. **152B**, 1 (1985).
[4] M. Ishikawa, S. Seki, K. Furuno, Y. Tagishi, M. Sawada, T. Sugiyama, K. Matsuda, T. Murayama, N. X. Dai, J. Sanada, and Y. Koike, Phys. Rev. C **28**, 1884 (1983).
[5] M. Bruno, F. Cannata, M. D'Agostino, M. L. Fiandri, M. Frisoni, H. Oswald, P. Niessen, J. Schulte-Uebbing, H. Paetz gen. Schieck, P. Doleschall, and M. Lombardi, Phys. Rev. C **35**, 1563 (1987).
[6] T. Rausch, H. Zell, D. Wallenwein, and W. v. Witsch, Nucl. Phys. **A222**, 429 (1974).
[7] M. Bruno, F. Cannata, M. D'Agostino, G. Vannini, M. Lombardi, and Y. Koike, Lett. Nuovo Cimento **29**, 385 (1980).
[8] N. O. Gaiser, S. E. Darden, R. C. Luhn, H. Paetz gen. Schieck, and S. Sen, Phys. Rev. C **38**, 1119 (1988).
[9] C. Werntz and F. Cannata, Phys. Rev. C **2**, 349 (1981).
[10] W. Grüebler, P. A. Schmelzbach, V. König, R. Risler, and D. Boerma, Nucl. Phys. **A242**, 265 (1975).
[11] D. Gola, W. Bretfeld, W. Burgmer, H. Eichner, Ch. Heinrich, H. J. Helten, H. Kretzer, K. Prescher, H. Oswald, W. Schnorrenberg, and H. Paetz gen. Schieck, Phys. Rev. C **27**, 1394 (1983).
[12] M. Karus, M. Buballa, J. Helten, B. Laumann, R. Melzer, P. Niessen, H. Oswald, G. Rauprich, J. Schulte-Uebbing, and H. Paetz gen. Schieck, Phys. Rev. C **31**, 1112 (1985).
[13] K. Wittlich, Diploma thesis, Universität Köln, 1991 (unpublished).
[14] P. Niessen, G. Rauprich, K. Wittlich, and H. Paetz gen. Schieck, Nucl. Instrum. Methods (to be published).
[15] G. G. Ohlsen, R. E. Brown, F. D. Correll, and R. A. Hardekopf, Nucl. Instrum. Methods **179**, 283 (1981).
[16] *Proceedings of the 3rd International Symposium on Polarization Phenomena in Nuclear Reactions,* edited by H. H. Barschall and W. Haeberli (University of Wisconsin Press, Madison, 1971), p. XXV.
[17] L. D. Knutson, Nucl. Phys. **A198**, 439 (1972).
[18] M. Bruno, F. Cannata, M. D'Agostino, M. L. Fiandri, M. Frisoni, G. Vannini, and M. Lombardi, Nucl. Phys. **A386**, 269 (1982).
[19] J. E. Bond and F. W. K. Firk, Nucl. Phys. **A287**, 317 (1977).
[20] Th. Stammbach and R. L. Walter, Nucl. Phys. **A180**, 225 (1972).
[21] D. J. Ernst, C. M. Shakin, and R. M. Thaler, Phys. Rev. C **8**, 507 (1973).
[22] J. Haidenbauer and W. Plessas, Phys. Rev. C **30**, 1822 (1984).

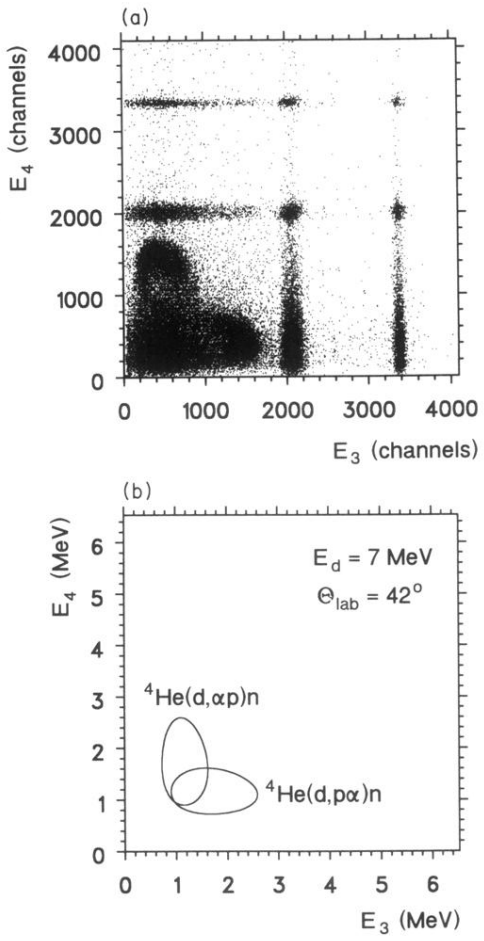

FIG. 1. Typical raw E_3-E_4 spectrum and the spectrum expected from kinematics, but without energy loss.

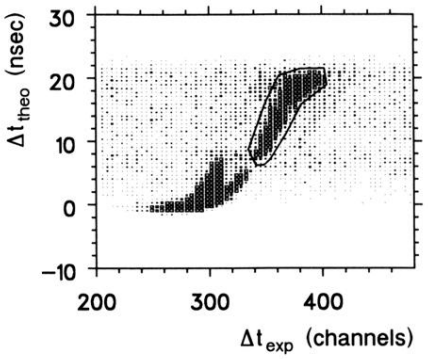

FIG. 3. Typical time-difference matrix with the area of the true p-α events marked by a polygon.